Chapter – 4

Texture Development in Ultrafine-Grained Low Carbon Steel

4.1 Macrotexture in Low Carbon Steel by ECAP

As-received low carbon steel ($\varepsilon_{vm} = 0$) has weak texture (Figure 4.1(a)). At the initial stage of deformation by ECAP [110] pole figure shows that individual components become gradually strong. At $\varepsilon_{vm} = 0.6$, the formation of weak components of $\{110\}_\theta$ fiber takes place with a maximum intensity of J_θ component (Figure 4.1(b), Table 4.1). Increasing strain to $\varepsilon_{vm} = 1.2$, the intensity of J_θ component enhances (texture intensity ~2.5) further with a slight change in the distribution of components of $\{110\}_\theta$ fiber (Figure 4.1(c)). At $\varepsilon_{vm} = 1.8$, no fiber texture is discernible and the intensities of J_θ and $D_{1\theta}$ components decrease (Figure 4.1(d)). On ECAP at $\varepsilon_{vm} = 3$, the intensity of F_θ, $\bar{E}_\theta$ and $D_{2\theta}$ components increase and form $\langle 111 \rangle_\theta$ fiber (Figure 4.1(e)).

At $\varepsilon_{vm} = 6$, the previously formed $\langle 111 \rangle_\theta$ fiber has got randomized and intensity of components J_θ, $\bar{J}_\theta$ and $D_{2\theta}$ are developed (intensity ~2) (Figure 4.1(f)). At $\varepsilon_{vm} = 9$, J_θ, $\bar{E}_\theta$ and $D_{2\theta}$ become strong (intensity ~3.2) (Figure 4.1(g)). At $\varepsilon_{vm} = 12$ - 16.8, J_θ, $D_{2\theta}$, and $\bar{E}_\theta$ components get strengthened, and after that, their intensities become strong (Figure 4.1(h)-(i), Table 4.1).

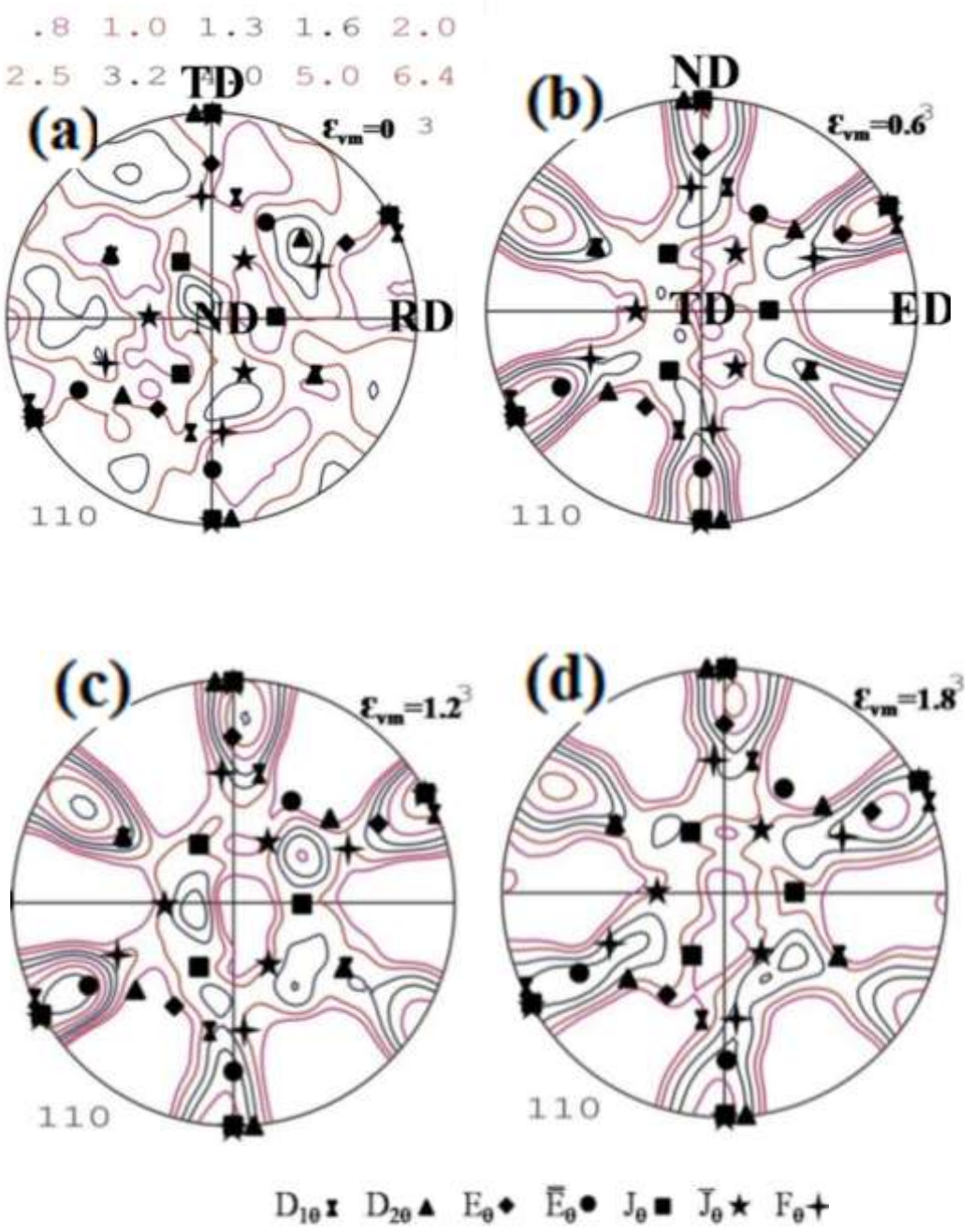

Figure 4.1: [110] pole figure maps of low carbon steel for (a) $\varepsilon_{vm} = 0$ and after ECAP for (b) $\varepsilon_{vm} = 0.6$, (c) $\varepsilon_{vm} = 1.2$, and (d) $\varepsilon_{vm} = 1.8$. RD, TD ND directions are denoted for as-received material and ED, TD ND directions are displayed on pole figures of ECAPed samples. Texture intensities 0.8, 1.0, 1.3, 1.6, 2.0, 2.5, 3.2, 4.0, 5.0, and 6.4 are projected.

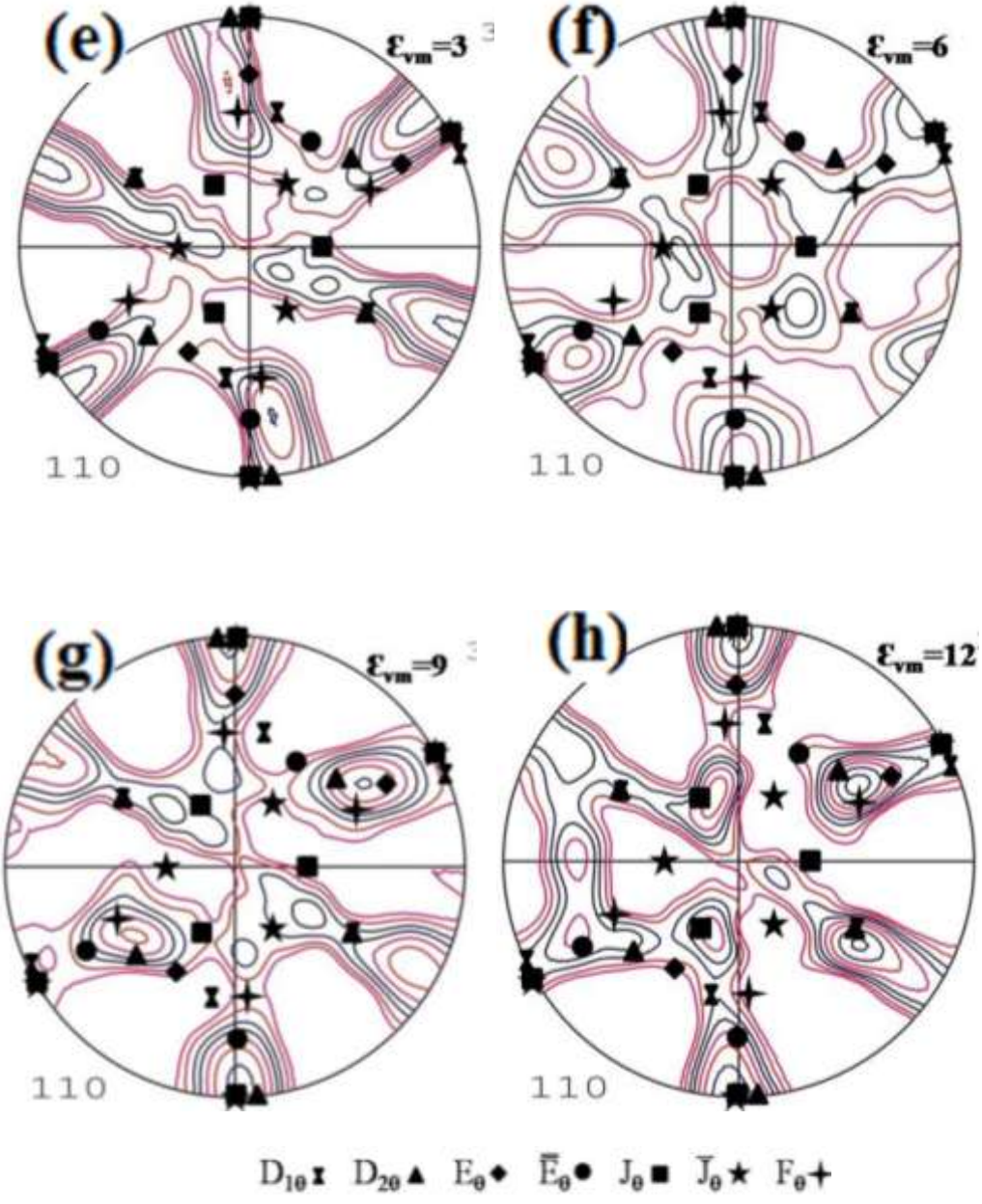

Figure 4.1: [110] pole figure maps of low carbon steel for (e) ε_{vm} = 3, (f) ε_{vm} = 6, (g) ε_{vm} = 9, and (h) ε_{vm} = 12.

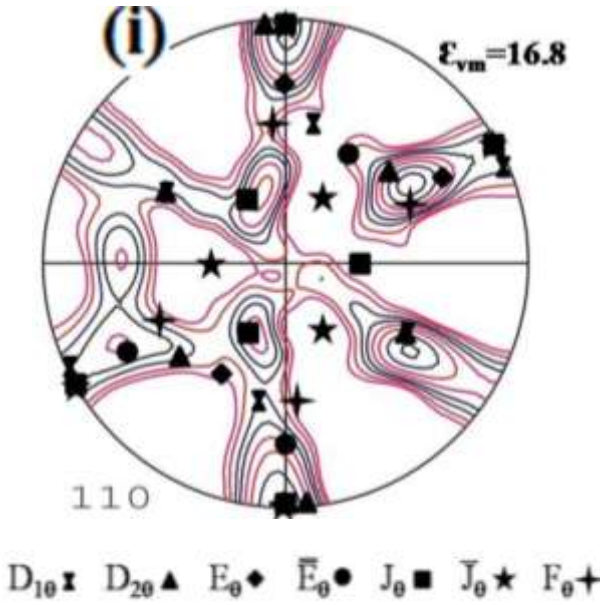

Figure 4.1: [110] pole figure maps of low carbon steel for (i) ε_{vm} = 16.8.

Table 4.1: Texture components in {110} pole figure of low carbon steel at various equivalent strains.

Equivalent strain (ε_{vm})	Texture Components						
	$\{110\}_\theta$ Fiber			Common Component		$\langle 111\rangle_\theta$ Fiber	
	F_θ	J_θ	$\bar{J}_\theta$	E_θ	$\bar{E}_\theta$	$D_{1\theta}$	$D_{2\theta}$
0	Overlapped	NA	NA	NA	NA	NA	exist
0.6	Overlapped	Appreciable	Low	NA	NA	Overlapped	NA
1.2	Overlapped	Appreciable	Low	NA	NA	Overlapped	NA
1.8	Overlapped	Low	NA	Low	NA	Overlapped	NA
3	Overlapped	NA	NA	NA	Appreciable	Overlapped	NA
6	Overlapped	Appreciable	Low	NA	Appreciable	Overlapped	Appreciable
9	Overlapped	Strong	NA	NA	Strong	Overlapped	Strong
12	Overlapped	Strong	NA	NA	Strong	Overlapped	Strong
16.8	Overlapped	Strong	NA	NA	Strong	Overlapped	Strong

Since single pole figures do not show intensity distributions of all the orientations, orientation distribution function (ODF) is calculated to predict an idea of exact orientation in φ_2= 45º section (Table 4.2). As-received material contains components F_θ, $D_{1\theta}$, $D_{2\theta}$, $\bar{J}_\theta$, however, their intensities are very low (intensity ~ 1.2) (Figure 4.2(a), Table. 4.2). For the ECAPed material possible ideal components are projected on respective ODF sections with enhanced φ_1 to φ_1+120º/2 and presented in the form of orientation distribution function, but major components are shown in φ_2 =45º section of ODFs (Figure 4.2).

On ECAP of low carbon steel at ε_{vm} = 0.6, the φ_2=45° ODF section is recorded with appreciable intensities of F_θ, J_θ, and $D_{1\theta}$ (Figure 4.2(b)). All the components begin to shift from their ideal position towards -φ_1 angle. At ε_{vm} = 1.2, re-evolution of J_θ, $D_{1\theta}$, $D_{2\theta}$ components takes place with $D_{2\theta}$ more intense than $D_{1\theta}$ (Figure 4.2(c)). Increase in strain to ε_{vm} = 1.8, results in weakening of most of the components (Figure 4.2(d)).

At ε_{vm} = 3, the intensity of components increases with a reduced spread as F_θ, $D_{2\theta}$, $\bar{J}_\theta$ form concentrated cloud and E_θ evolves. These components are still shifted towards -φ_1 angle (Figure 4.2(e)).

At ε_{vm} = 6 intense $D_{2\theta}$ is formed (intensity ~ 5) and is the stage of transformation in the intensity of components, where J_θ, $\bar{J}_\theta$ are also dominating (intensity ~3), components along with the reduced intensity of E_θ component (Fig. 5(f)). At ε_{vm} = 9, $\langle 111 \rangle_\theta$ fiber components $D_{1\theta}$, $D_{2\theta}$ are consolidated (Figure 4.2(g)). Further deformation (ε_{vm} = 12 - 16.8) leads to an increase in the intensity of $D_{1\theta}$ (intensity ~ 7.5) along with strong components of E_θ (Figures 4.3(h, i)). However, E_θ shifted appreciably towards the positive φ_1 direction. A new texture component E_θ appears at high equivalent strain (> 9) with high intensity which is absent in IF steel.

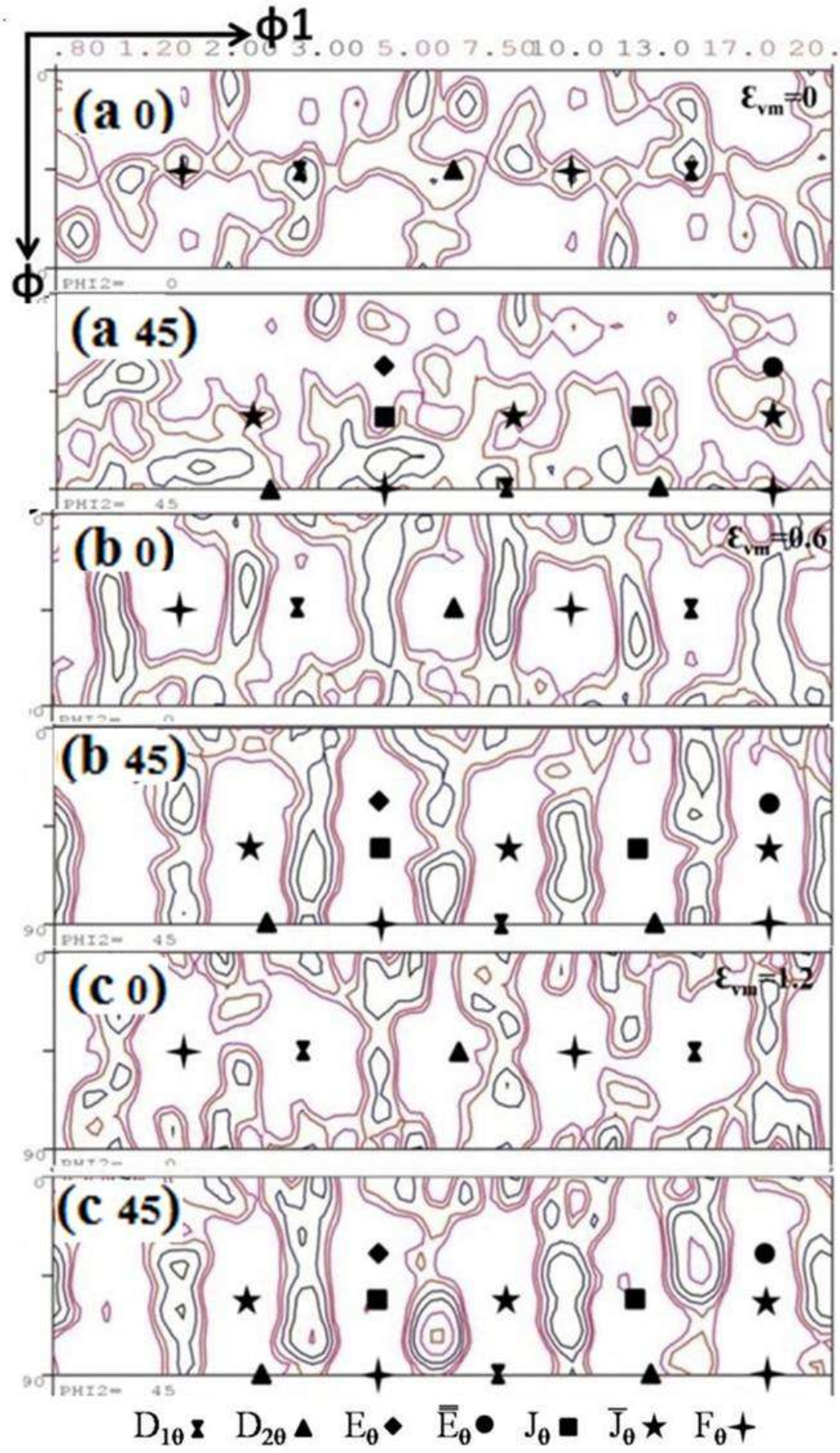

Figure 4.2: φ_2=0° and 45º sections of ODF maps of low carbon steel for (a0, a45) ε_{vm} = 0 and after ECAP for (b0, b45) ε_{vm} = 0.6, (c0, c45) ε_{vm} = 1.2. Texture data is rotated such that φ_1 becomes φ_1+120º/2 towards negative simple shear. Texture intensities are 0.8, 1.2, 2.0, 3.0, 5, 7.5, 10, 13, 17, 20.

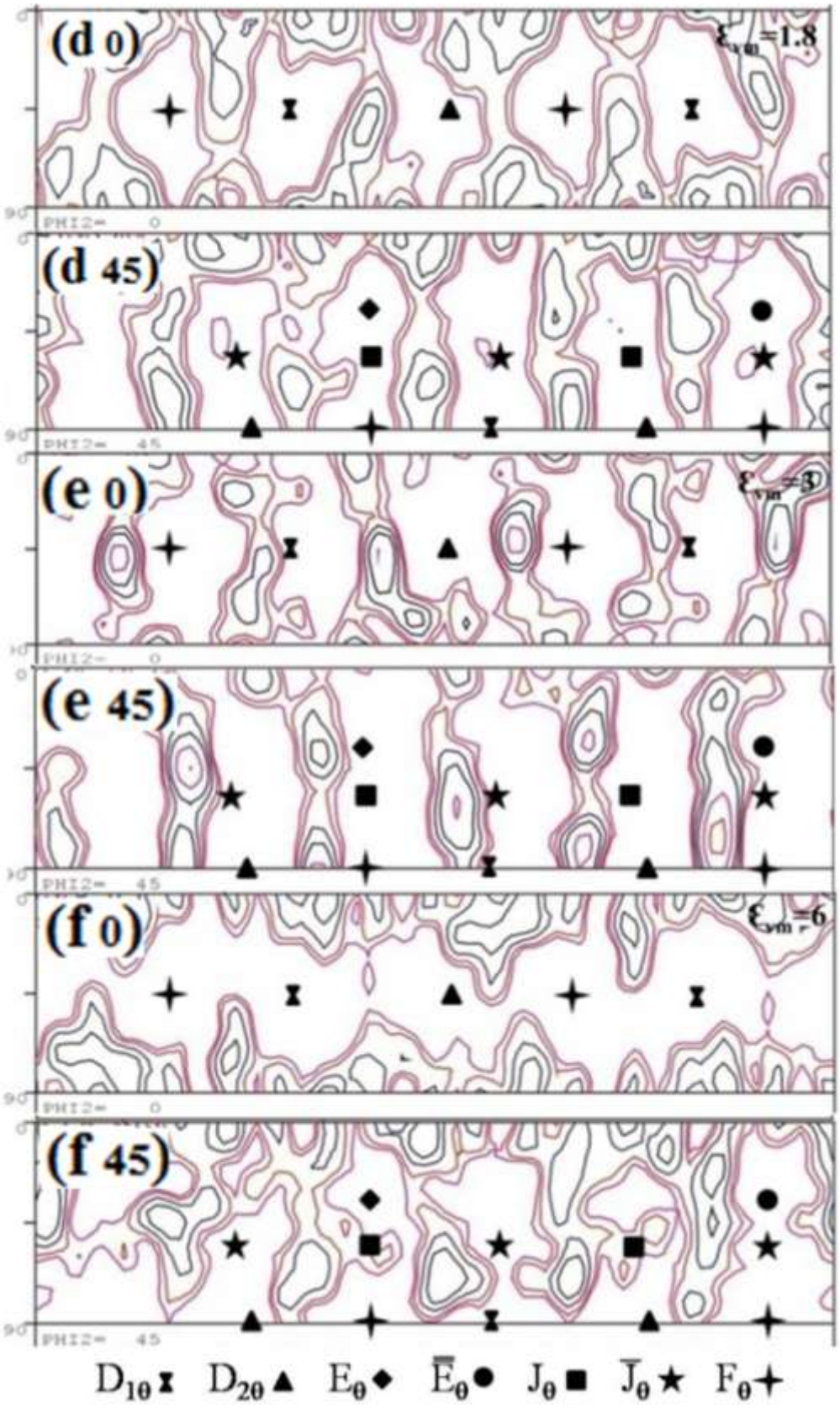

Figure 4.2: φ_2=0° and 45º sections of ODF maps of low carbon steel for (d0, d45) ε_{vm} = 1.8, and (e0, e45) ε_{vm} = 3, and (f0, f45) ε_{vm} = 6.

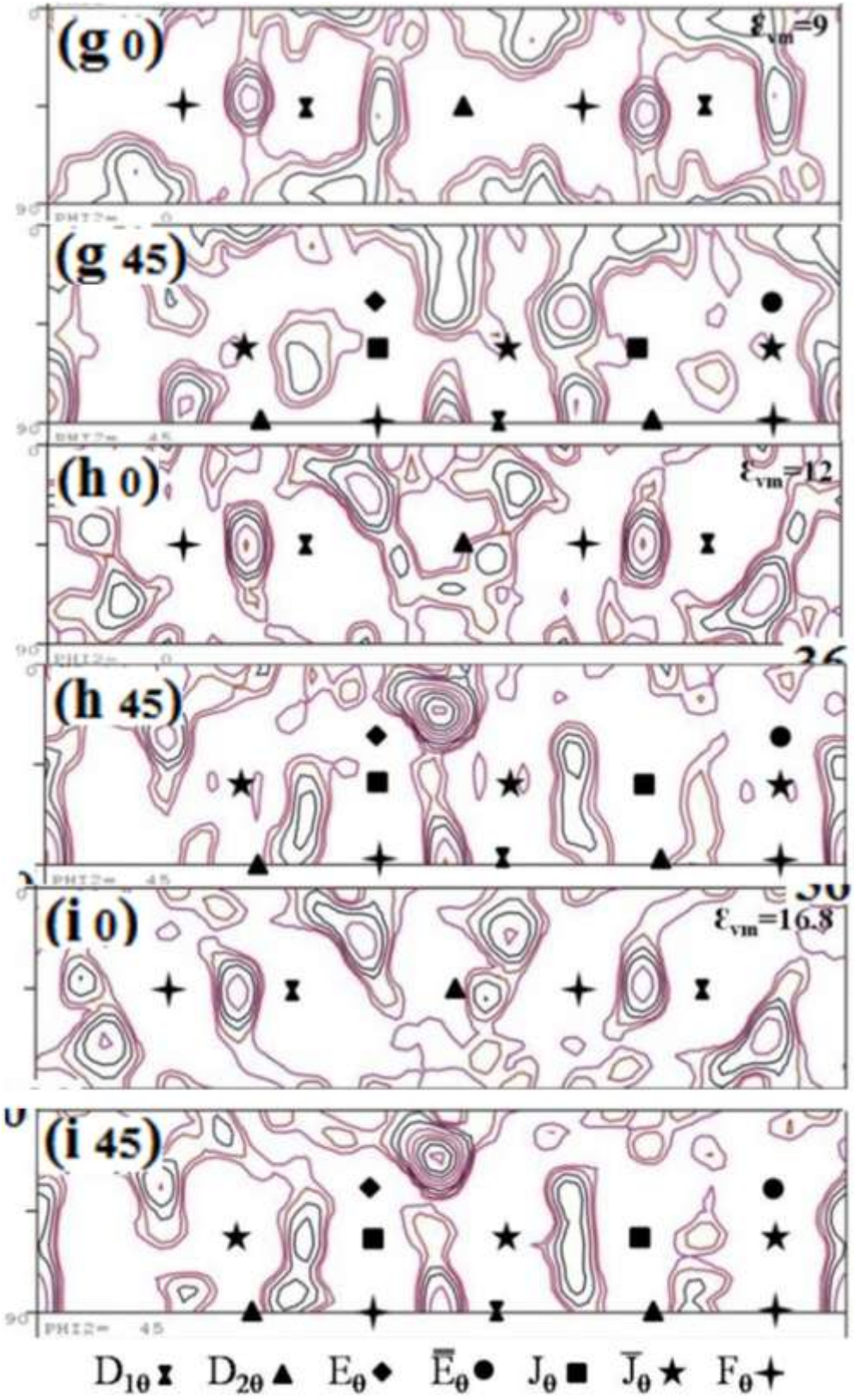

Figure 4.2: φ2=0° and 45º sections, ODF maps of low carbon steel for (g0, g45) ε_{vm} = 9, (h0, h45) ε_{vm} = 12, and (i0, i45) ε_{vm} = 16.8.

Table 4.2: Texture intensity of important texture components of low carbon steel in ODFs of φ_2=0° and 45° with equivalent strain.

Equivalent strain	Texture Intensity					
	$\{110\}_\theta$ Fiber Components			Common Component	$\langle 111\rangle_\theta$ Fiber Components	
	F_θ	J_θ	$\bar{J}_\theta$	E_θ	$D_{1\theta}$	$D_{2\theta}$
0	1.2	1.2	1.2	0	1.2	0
0.6	3	3	3	0	3	0
1.2	5	3	0	1.2	7.5	3
1.8	2	1.2	0.8	0	1.2	2
3	7.5	0	5	3	5	3
6	1.2	3	3	1.2	3	5
9	0	2	0.8	3	5	5
12	0	3	0.8	17	7.5	3
16.8	1.2	3	1.2	17	5	3

The as-received low carbon steel has low texture index (Figure 4.3). Upon ECAP texture index increases at a rapid rate at low strain level (ε_{vm} = 0 - 1.2) and reaches a value as high as 2.48 at ε_{vm} = 1.2.

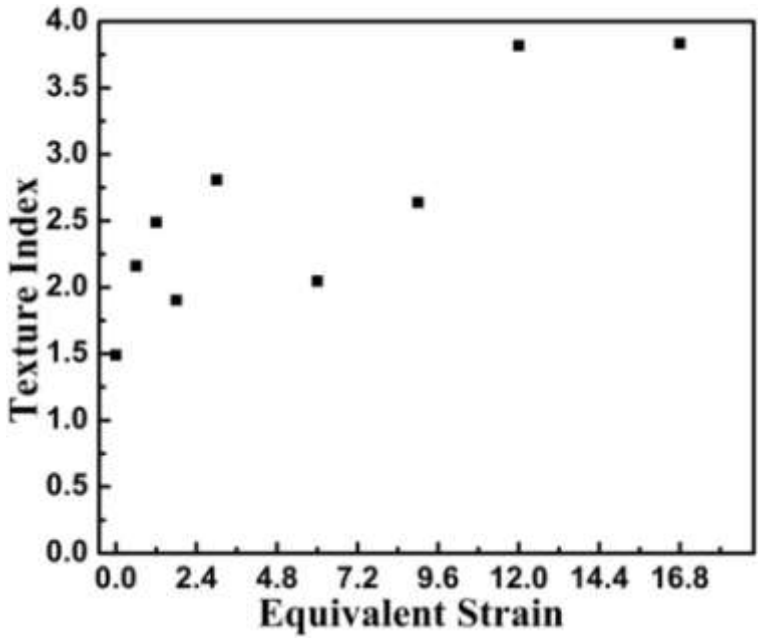

Figure 4.3: Variation of texture index with equivalent strain.

On further straining the texture index fluctuates in the strain regime decreases to ε_{vm} = 1.8-3. Beyond ε_{vm} = 6 the texture index increases at a low rate and reaches a saturated value of 3.81 at ε_{vm} = 12. After that texture index maintains the value at least up to ε_{vm} = 16.8.

Table 4.3: Deviation of Components from ideal positions in ECAPed low carbon steel.

	Texture intensity					
	$\{110\}_\theta$ Fiber Components			Common Component	$\langle 111\rangle_\theta$ Fiber Components	
Equivalent strain	F_θ	J_θ	$\bar{J}_\theta$	E_θ	$D_{1\theta}$	$D_{2\theta}$
0						
0.6	-29	-25			-25°	
1.2		-25				
1.8		-25			-25	-29
3	-18				-8	-28
6						
9					-16	-25
12				+25	-18	+15
16.8				+25	-18	+15

Deviations of components from ideal positions in the φ_2 =0 and 45° sections of ODFs for low carbon steel are shown in Tables 4.3. Deviations of components from ideal positions for similar section of ODFs are taken from the reference [Verma et al. 2016] and displayed in Table 4.4.

Texture components of low carbon steel are deviated more when compared to the same components of IF steel processed under identical conditions (i.e., routes. equivalent strain, etc.) at low to intermediate strain (equivalent strain < 9). The deviation of components from their ideal position in the case of low carbon steels decrease at high equivalent strain level but, in the case of IF steel, the deviations continue to increase at a low rate with increase in equivalent strain.

Table 4.4: Deviation of Components from ideal positions in ECAPed IF steel [Verma[a] et al. 2016].

	Deviation of Position of components with respect to Φ1					
	$\{110\}_\theta$Fiber Components			Common Component	$\langle 111\rangle_\theta$ Fiber Components	
Equivalent strain	F_θ	J_θ	$\bar{J}_\theta$	E_θ	$D_{1\theta}$	$D_{2\theta}$
0.6		exact	exact		-22°	-32°
1.2	exact		exact			-23
1.8		exact	exact		-23	-41
2.4	-23	exact	exact		-32	-23
3	exact	-23	exact		-27.6	-41
6	-25	+18.4	exact		-30	+9.2
9	exact	+4.6	exact		-23	+9.2
15	+4.6	-4.6	exact		-13.8	-27.6
21	exact	+18.4	exact		exact	+4.6
16.8	exact	exact	exact		-13.8	+13.8

4.2 Discussion

The texture strength of the ECAPed LCS increases continuously with increasing imposed strain range ε_{vm} = 0.6 - 1.2 due to grain subdivision to bands and

grain rotation towards stable orientation. With further increase in strain the index decreases due to randomization, i.e., reorientation of bands. The decrease in texture strength at ε_{vm} = 1.8 is related to resistance to change in simple shear texture [Beyerlein et al. 2003]. Splitting of bands into cells by the recovery of dislocations leads to randomisation. If initial texture index is high, there is a tendency to randomize in the next pass and texture strength is weakened [Beyerlein et al. 2009]. At ε_{vm} = 3, fragmentation of bands due to strain reversal process takes place which results in a slight increase of texture index and strengthening of already formed $\bar{J}_{\theta}$, F_{θ}, $D_{1\theta}$ and $D_{2\theta}$ texture components. At this ε_{vm} evolution of E_{θ} component also takes place. The bands also get aligned towards the direction of deformation with increasing strain [Verma[b] et al. 2016] leading to increased texture strength.

At ε_{vm} = 6, lamellar structures are formed by the alignment of the high angle boundaries of deformation bands and a few cell block boundaries as well get oriented towards the deformation direction and result in a decrease of texture index as cells and grains rotate in macroscopic deformation direction and attain new orientations. The intensity of (110)[112] component decreases consequently. Therefore, texture strength is maintained due to an increase in the intensity of J_{θ} component. After ε_{vm} = 9, the material is strongly textured. The width of lamellar boundaries decreases to a few subgrains-wide, their aspect ratio increases at ε_{vm} = 12. There is inhomogeneity in the microstructure as both ribbon and nearly-equiaxed grains exist at ε_{vm} = 12 with diffuse boundaries. The fraction of near-equiaxed grains with diffused boundaries is increased at ε_{vm} = 16.8. The presence of diffuse boundaries gives a signature of non-equilibrium nature of the boundaries. Moreover, the presence of extinction contours also confirms a severely strained state of the material. Texture index continuously increases even after ε_{vm} = 12, but major texturing is due to the formation of J_{θ}, E_{θ}, $D_{1\theta}$,

and $D_{2\theta}$ components. The texture strength is nearly unchanged above ε_{vm} = 12 at least up to ε_{vm} = 16.8. This static state does not mean that grains have rotated to a stable orientation but only indicates that they became very similar due to the repetition of deformation path [Beyerlein et al. 2009].

There is a high fraction of the low angle grain boundaries (LAGBs) at the initial stage of deformation which later transforms into a high fraction of high angle grain boundaries (HAGBs) due to the repeated cycles of deformation. There exists a large amount of structural inhomogeneity at the high angle boundaries. The crystal lattice gets expanded locally at the interface to accommodate the structural mismatch due to a destruction of perfect crystal and introduction of grain boundaries into a stack of lattice planes [Wolf et al. 1989].

The texture components {110}[001] (F_{θ}) and {110}[112] (J_{θ}) evolve formed at initial stage of deformation (ε_{vm} = 0.6 - 3). {112}[111] (D_{θ}) orientation is relatively difficult to slip. Thus, the (D_{θ}) orientation can be anticipated as the stable orientation which is also in agreement with the increase in the intensity of the {112}[111] (D_{θ}) type textures in the high strain range of ε_{vm} = 9 - 16.8 range. It is inferred to be due to the further slipping behavior. After that, a minimum number of grains attain D_{θ} orientation at a low ε_{vm} level and remain stable up to high ε_{vm} level. Moreover, new grains also begin to attain {112}[111] orientation for stability leading to an increase in the intensity of this component with strain. At high strain level (ε_{vm} = 9 - 16.8), the material gets refined and strengthened with applied equivalent strain. At that condition operative slip system requires higher stresses, which are the cases for D_{θ} and E_{θ} orientations/slip systems and therefore their intensities get enhanced.

The strain path influences the deviation of texture components from their ideal position strongly. If a material is ECAPed via route Bc, where the sample is rotated

90° always in one direction with respect to the axis of the sample (either in clockwise or anti clockwise) between two consecutive passes, the shear plane changes after each pass and a sample with a new texture is inserted in the die. This leads to deviation of the texture components from their ideal positions in the sample that has undergone more than one pass [Li et al. 2006]. The reported maximum deviations are as high as 20° [Gazder et al. 2006]. The initial texture and intersection plane of the die can cause deviation of texture from ideal position [Ferrasse et al. 2004]. Initially imposed strain is low but deviation angle is high which may have the effect of both initial texture and low imposed strain, as strain will not be sufficient to align a good number of grains with the shear plane and direction. Moreover, initially material has a low intensity texture component which also will resist change of orientations of grains at $\varepsilon_{vm} = 0.6$ and thus deviate the components from their ideal positions. After the first pass, fragmentation processes continue and slowly force texture components to align with shear plane and directions.

Deformation is homogeneous, and uniform throughout the work piece if friction between the work piece and die is negligible [Beyerlein et al. 2009, Gazder et al. 2006]. Friction reduces deformation close to the surface of the workpiece. In the present case, friction has been reduced by using a lubricant and the sample selected for texture study is from the center of the workpiece. Therefore the friction effect for deviation of ideal texture component can be neglected. The inner intersection angle of the die is zero, but outer arc angle is 60º. This is contributing significantly for deviation of texture components from their ideal position. Therefore, a significant deviation is observed even at $\varepsilon_{vm} = 0.6$. The deviation can also arise from the role played pearlitic cementite on homogeneous deformation as large pearlite colonies are scattered at the initial stage of deformation which hinder the ferrite grains to orient in

the direction of deformation. However, at the high ε_{vm} level, pearlite colonies get broken down, and cementite gets partially dissolved. This dissolution reduces the resistance to deformation of ferrite, and therefore the deviation angle is reduced for components that form at a high strain.

IF steel contains very low amount of carbon (> 0.0038). The carbon is scavenged from the interstitial positions by Ti or Nb, and very small amount of respective carbides are formed. Thereby, the steel becomes interstitial free. The low carbon steel differs from the IF steel by the presence of about 10% pearlite as both the materials in as-received condition contain weak texture and this effect get eliminated by ECAP in the range ε_{vm} = 0.6 to 2.4. The formation of texture components and their intensities in low carbon steel differ by the presence of 10% pearlite. The presence of pearlite at low to intermediate strain (ε_{vm} = 9) strongly influence the texture of low carbon steel. Therefore, the components deviate more from the ideal position in low carbon steel than in the case of IF steel processed in the range of $\varepsilon_{vm} < 9$. Beyond ε_{vm} = 9, part of pearlite gets dissolved, and therefore, deviations of components in low carbon steel from the ideal position in the φ_2 = 45° section of ODFs are lower in comparison with IF steel [Verma[a] et al. 2016]. The presence of pearlite facilitates the formation of texture component E_θ at high strain which is absent in IF steel even at very high strain (ε_{vm} = 24) [Verma[a] et al. 2016].

4.3 Summary

Microstructure and texture evolution in low carbon steel under shear strain is investigated systematically in the strain regime ε_{vm} = 0-16.8.

1. At initial strain level (ε_{vm} = 0.6 - 1.2), low carbon steel gets textured due to grain subdivision into bands. At intermediate strain (ε_{vm} = 3 - 6), the material is strongly

textured due to alignments of bands though it fluctuates due to randomization of initial strong texture. At high strain level (ε_{vm} = 9 - 16.8) texture is randomized due to breakage of ribbon grains into near-equiaxed structure resulting in a decrease in the rate of increase in texturing with respect to strain, though the texture intensities at different strains are enhanced and reach a saturation level at ε_{vm} = 12.

2. ECAP of low carbon steel forms F_θ (110)[001], J_θ (110)[$1\bar{1}2$], $\bar{J}_\theta$ ($\bar{1}\bar{1}0$)[$\bar{1}1\bar{2}$] and $D_{1\theta}$ ($\bar{1}\bar{1}2$)[111] at low strain range (ε_{vm} = 0.6 - 1.2). At intermediate strain range (ε_{vm} = 3 - 6), F_θ , $\bar{J}_\theta$, and D1θ get strengthened, and new component $D_{2\theta}$ ($11\bar{2}$)[111] is also formed. At high strain range (ε_{vm} = 9 - 16.8), intensities of $D_{1\theta}$, $D_{2\theta}$ are maintained, but new component E_θ (110)[$1\bar{1}1$] also appears and becomes intense. There was no texture symmetry in the pole figures or in the ODFs as the sample gets rotated through non-symmetric texture axis between successive passes of ECAP (strain path Bc).
3. The presence of pearlite strongly influences the deviation of texture components from their ideal position at $\varepsilon_{vm} < 9$, and the deviation gets reduced at a high strain level $\varepsilon_{vm} > 9$ due to partial dissolution of pearlitic cementite. The texture intensity continues to increase with induced equivalent strain. The pearlitic carbide further enhances the intensity. However, partial dissolution of the carbides lowers the increase in the texture index. The pearlitic carbides allow the formation of E_θ component at $\varepsilon_{vm} > 3$ whose intensity reaches a maximum value of 17 at ε_{vm} = 12, whereas, E_θ component is absent in IF steel even at ε_{vm} = 24.